JOURNAL OF ROCK MECHANICS
VOL. 9, NO. 4, PP. 33-43.
https://doi.org/10.22034/IRSRM.2026.578065.1075

# Comparison of the RHT and KCC Constitutive Models Performance Under static and Quasi-Static Loading Conditions for Jinping Marble

**Hooman Rouhani[1], Aida Ameli Ghamsar[1], Ebrahim Farrokh[1*]**
**1. Department of Mining Engineering, Amirkabir University of Technology, Tehran, Iran.**

**Received: 21 January 2026 Accepted: 20 March 2026**
**(*Corresponding author: e.farrokh@aut.ac.ir)**

**Keywords**
**Constitutive model**
**RHT**
**KCC**
**Jinping marble**

**Abstract**

This study evaluates and compares the predictive performance of the RHT and KCC constitutive models in simulating the mechanical behavior of Jinping marble. First, the constitutive models, including the strength criteria and equations of state of each model, are briefly introduced. Subsequently, the model parameters required to predict the static behavior of marble under triaxial stress states are determined. Using both constitutive models, triaxial compression tests were numerically simulated at confining pressures of 5, 20, and 40 MPa, and the simulation results were compared with corresponding laboratory data. The results demonstrate that the RHT constitutive model provides better predictions of peak strength and pre-failure behavior than the KCC model. Accordingly, the RHT model was selected as the preferred constitutive formulation, and its post-failure response was further calibrated to improve agreement with the experimental observations.

## I. INTRODUCTION

The relations and governing equations that describe the relationships among the aforementioned variables for rock and other engineering materials are collectively referred to as constitutive models [1]. For the first time, Johnson and Holmquist (1992) proposed the JH-1 constitutive model to simulate the behavior of brittle materials such as ceramics, incorporating the effects of strain rate and confining pressure on material strength [2]. The model was developed to predict material failure, post-failure strength degradation, and large deformations. However, after implementation in various numerical simulation codes, some limitations were identified in predicting post-peak softening behavior. To address these deficiencies, the same authors proposed the JH-2 model as an advanced formulation, widely applied to brittle and quasi-brittle materials, which was subsequently implemented into various numerical simulation platforms [3]. The JH-2 model parameters were later determined for granites and red sandstones in 2006 and 2021, respectively [4], [5]. Moreover, JH-2 has been extensively employed in various rock mechanics and engineering analyses [6-11]. In a related development, the JHC model was proposed by Johnson, Holmquist, and Cook in 1993 for simulating concrete under high strain rates, elevated confining pressures, and large deformations [12]. The parameters of the JHC model were later determined for both dolomite and coal by several researchers, and the numerical simulations were compared taken with the results of laboratory tests [13,14]. In addition, the JHC model has been used by several researchers to simulate various rock engineering problems [15,16]. As mentioned earlier, these constitutive models capture the effects of the strain rate and confining pressure on the strength of brittle, semi-brittle materials like rock and concrete. However, in all of the aforementioned models, the failure surface was expressed in two dimensions and did not address the impact of the intermediate principal stress. Hence, they cannot actually model true triaxial stress conditions. This limitation motivated researchers at the Karagozian & Case Institute to develop the KCC constitutive model in 1996 and 1997. The model is capable of representing true triaxial stress conditions and predicting rock strength through a fully three-dimensional failure surface [17,18]. Similar to the JH-2 and JHC models, the KCC model was initially developed for concrete. Later, its parameters were calibrated for dolomite and

sandstone and reported in 2020 and 2019, respectively [19,20]. Tian et al. (2022) and Mardalizad et al. (2020) simulated and analyzed the rock cutting process using the KCC model [21,22]. Kucewicz et al. compared three constitutive models, namely JH-2, JHC, and KCC, by benchmarking numerical simulation results against experimental data from spherical projectile impact tests on dolomite blocks, small-scale blast tests, and Hopkinson pressure bar tests. According to the comparative results of Kucewicz et al., both the JH-2 and KCC models generally provided superior predictions. However, it should be noted that the KCC model overestimates the spatial extent of the damaged zone, whereas the growth and propagation of cracks—as well as the overall damage distribution—are predicted more accurately by the JH-2 model [23]. Riedel, Thoma and Hiermaier (1999) presented the RHT constitutive model for simulating the mechanical behavior of concrete. The RHT model can excellently capture the response of concrete and other brittle materials for a wide range of strain rates, very high confining pressures, and true triaxial stress states. In addition, the model computes post-peak strength by interpolating between different strength levels, corresponding to the material damage and stress state at each instant [24,25]. Rouhani and Farrokh (2024) suggested a systematic methodology for determination, calibration, and verification of the RHT model parameters for Nehbandan granite [26]. There appears to be a noticeable gap in the literature regarding a systematic comparison of constitutive models that are capable of predicting the strain-rate-dependent behavior of rocks under three-dimensional (3D) stress states, including their post-peak response. Such a comparison is currently lacking and is needed to guide model selection for rock dynamics applications.

In this paper, the RHT and KCC models are briefly introduced and the model parameters for Jinping marble are determined. Finally, the predictive performance of these two models in simulating the behavior of Jinping marble under various confining pressures is assessed.

## II. Material Description and Constitutive Models

### *A.* Material Description

The rock selected for numerical simulation in this study is Jinping marble. Rock samples were collected from Sichuan Province, China. The mechanical behavior of Jinping marble under conventional triaxial stress state has been investigated by several researchers [27-29].

In this study, to simulate the models using the RHT and KCC models, the physical properties (density and porosity), uniaxial compressive strength, Young's modulus, Poisson's ratio, and tensile strength were adopted from the literature. The failure surface parameters were determined from the triaxial compressive strength test results of Jinping marble reported in the literature. The equation of state parameters were calculated based on Young's modulus and Poisson's ratio. Furthermore, the true triaxial test results investigated by several researchers on marble specimens were utilized to generate the parameters that define the third invariant of the deviatoric stress tensor.

### *B. KCC Constitutive Model*

The failure function of the Karagozian and Case (KCC) constitutive model in LS-DYNA is defined by a pressure-sensitive yield surface, $\phi$ (ρ, θ, ξ, λ), given in Eq. (1) in terms of the Haigh–Westergaard stress invariants [20].

$$\phi\,(\rho,\theta,\xi,\lambda) = \sqrt{3/2}\;\rho - \varphi(\theta,\xi,\lambda) \tag{1}$$

Where: $\lambda$ denotes the damage parameter and $\varphi(\theta,\xi,\lambda)$ is the yield function of the KCC constitutive model. $\rho$, $\theta$ and $\xi$ are the quantities related to the Haigh–Westergaard coordinate system and are defined according to Eq. (2) [20].

$$\begin{cases} \xi = \sqrt{3}\,p = I_1/\sqrt{3} \\ \rho = \sqrt{2J_2} = \sqrt{2/3}\,\sigma_{eq}\;\left(\sigma_{eq} = q\right) \\ \cos(3\theta) = (r/q)^3 = 3\sqrt{3}J_3/2J_2^{3/2} \end{cases} \tag{2}$$

Where: $I_1$denotes the first invariant of the stress tensor, and $J_2$ and $J_3$ represent the second and third invariants of the deviatoric stress tensor. Furthermore, the KCC model's yield function, yield, peak, and residual strength surfaces, as well as its damage model, are subsequently presented [20]. As previously discussed, the KCC model comprises three fixed failures surfaces which are: 1) the yield strength surface, 2) the ultimate or peak strength surface, 3) the residual strength surface. Each of these surfaces is calculable using Eq. (3)-(5), as determined from the results of triaxial compression tests [20].

$$\sigma_y(p) = a_{o_y} + \frac{p}{a_{1_y} + a_{2_y}p} \tag{3}$$

$$\sigma_m(p) = a_o + \frac{p}{a_1 + a_2 p} \tag{4}$$

$$\sigma_r(p) = \frac{p}{a_{1_f} + a_{2_f}p} \tag{5}$$

Eq. (3)-(5) can also be written in $\xi - \rho$ system as follows:

$$\rho_y = \sqrt{2/3}\,a_{o_y} + \frac{\sqrt{2}\xi}{3a_{1_y} + \sqrt{3}a_{2_y}\xi} \tag{6}$$

$$\rho_m = \sqrt{2/3}\,a_o + \frac{\sqrt{2}\xi}{3a_1 + \sqrt{3}a_2\xi} \tag{7}$$

$$\rho_r = \frac{\sqrt{2}\xi}{3a_{1_f} + \sqrt{3}a_{2_f}\xi} \tag{8}$$

Where: the coefficients $a_i\,(i = 0, 1, 2)$ can be determined through curve fitting based on the results of

triaxial compression tests. Additionally, $y$, $m$ and $r$ denote the yield, peak and residual states. As shown in Fig. 1, the overall configuration of the strength model within the KCC constitutive framework is illustrated on both the meridian and deviatoric planes.

In Fig. 1, P*, $\Delta\sigma$ and θ represent the normalized mean stress (relative to the unconfined compressive strength), the deviatoric stress, and the lode angle, respectively. Furthermore, r(θ) is the radial distance from the hydrostatic axis in deviatoric plane. Additionally, $r_c$ and $r_t$ represent the radial distance from the hydrostatic axis to the failure surface along the compressive meridian and the tensile meridian, respectively.

According to Fig. 2, the KCC constitutive model parameters were determined using triaxial compression test results obtained by Jiang et al. (2016) on Jinping marble [27]. Based on the calibrated coefficients listed in Table 1, the yield, peak and residual strength surfaces for Jinping marble were plotted and are presented in Fig. 2. As shown in Fig. 2, the interpolated strength curves predicted by the KCC constitutive model are in good fit with the experimental results.

The KCC constitutive model represents the elastic deformation of rock through its equation of state and the Poisson's ratio. The equation of states describes the relationship between mean stress and volumetric strain, or the ratio of the current to initial volume. Based on elasticity theory and Hooke's law, the relationship between mean stress and volumetric strain is characterized by the bulk modulus and can be expressed linearly as: $p = K\mu$. In this equation, $p$ denotes the mean stress, $\mu$ represents the volumetric strain, and $K$ is the bulk modules. In this study, due to the lack of certain experimental data, the Poisson's ratio and Young's modulus of Jinping marble were employed to calculate the bulk modulus using Eq. (9). The Poisson's ratio and Young's modulus of Jinping marble are taken as 0.25 and 55 GPa, respectively. Accordingly, regardless of the nonlinear behavior of the equation of state, the elastic behavior of Jinping marble is defined linearly in the numerical model.

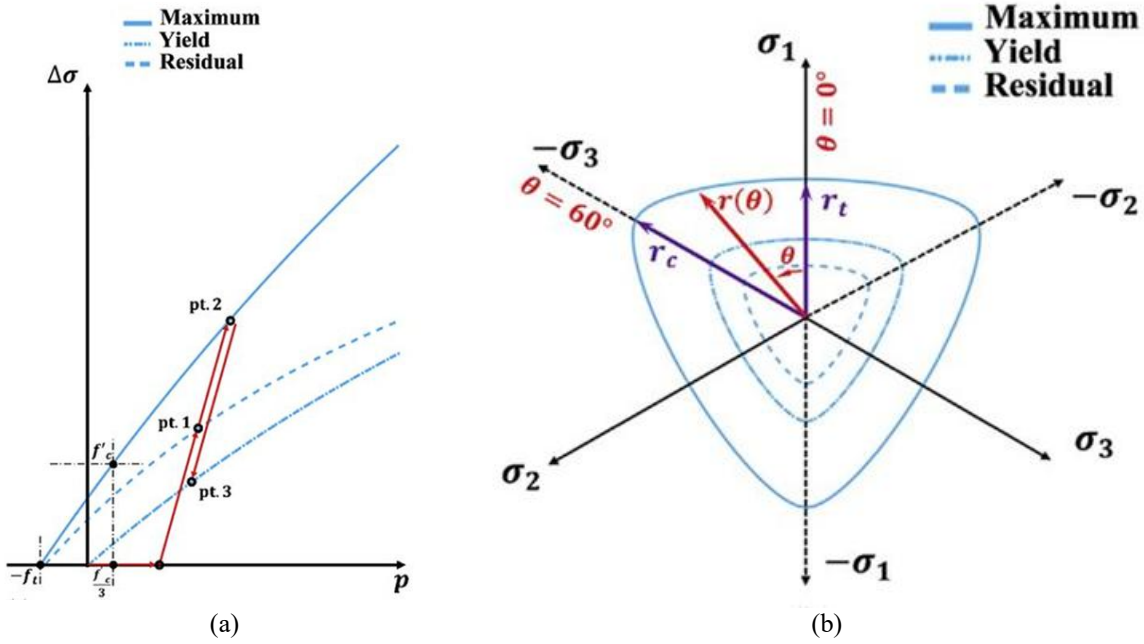


**Fig 1. (a) Interpolation in a linear fashion across the failure envelopes, (b) Deviatoric plane formulation introduced in the Willam–Warnke model** [20]**.**

**Table 1. Calibrated strength-surface parameters of the KCC constitutive model for Jinping marble.**

| Surface | Parameter | Value | $R^2$ (%) |
|---|---|---|---|
| yield surface | $a_{oy}$ | 18.15 | 98.96 |
| | $a_{1y}$ | 0.1336 | |
| | $a_{2y}$ | 0.008337 | |
| Peak strength surface | $a_o$ | 52.95 | 99.99 |
| | $a_1$ | 0.589 | |
| | $a_2$ | 0.001096 | |
| Residual strength | $a_{of}$ | 0.4669 | 99.53 |
| | $a_{1f}$ | 0.001092 | |

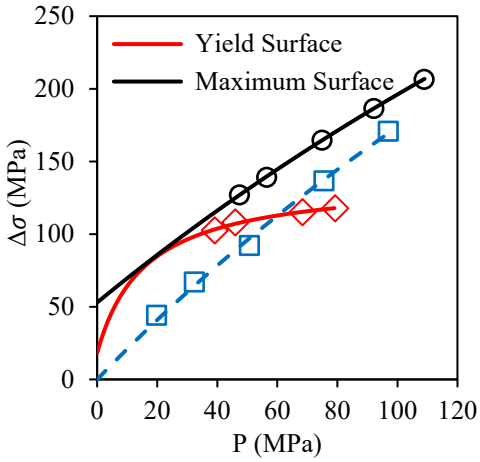


**Fig 2. Strength surfaces of the KCC constitutive model for Jinping marble.**

$$K = \frac{E}{3(1-2\upsilon)} \tag{9}$$

*C. RHT Constitutive Model*

The RHT model is another constitutive model developed by Riedel, Hiermaier, and Thoma in 1999 to predict the behavior of concrete under high confining pressure and high strain rates, while accounting for the true triaxial stress state of rock and concrete. The RHT model features three failure surfaces: the elastic limit surface, the residual strength surface, and the failure (or peak strength) surface. The peak strength and elastic limit surfaces are functions of the intermediate principal stress (or the third invariant of the deviatoric stress tensor) and the Lode angle. However, the residual strength surface is independent of the Lode angle and has a conical shape; in each deviatoric plane, the distance from the mean stress axis to any point on the surface is assumed to be identical. Fig. 3 schematically presents the RHT failure surfaces [26].

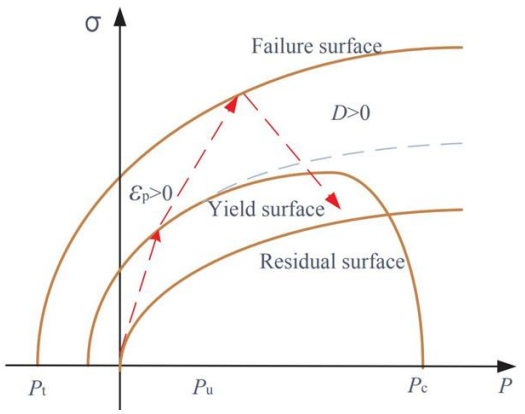


**Fig 3. RHT Constitutive Model Strength Surfaces [24].**

According to the failure surfaces, the yield function corresponding to the maximum strength surface $\sigma_f^*$ and the residual strength surface $\sigma_r^*$ for the RHT model are given by Eqs. (10) and (11) [31].

$$\sigma_f^* = A\,(p^* - \frac{F_R}{3} + (\frac{A}{F_R})^{-(1/n)})^n \tag{10}$$

$$\sigma_r^* = A_f p^{*N_f} \tag{11}$$

Where: $A$ and $n$ are the parameters associated with the peak strength failure surface of the RHT constitutive model. The quantities $A_f$ and $N_f$ are the coefficients related to the residual strength surface. The parameter $F_R$ represents the dynamic increase factor relative to the corresponding static strength at different strain rates.

As shown in Fig. 3, the horizontal and vertical axis represent the mean stress and the deviatoric stress ($\sqrt{3J_2}$), respectively, both of which are normalized with respect to the uniaxial compressive strength.

As discussed earlier, the peak strength surface of the RHT constitutive model is a three-dimensional, and its projection onto the deviatoric plane is not circular. Indeed, the peak strength surface shown in Fig. 3 is the only compressive meridian of Jinping marble. To obtain the full three-dimensional surface, the RHT constitutive model provides a linear relation that expresses the ratio of the tensile meridian to the compressive meridian, as given by Eq. (12). The parameters A, n, $A_f$, and $N_f$ were determined according to Fig. 4.

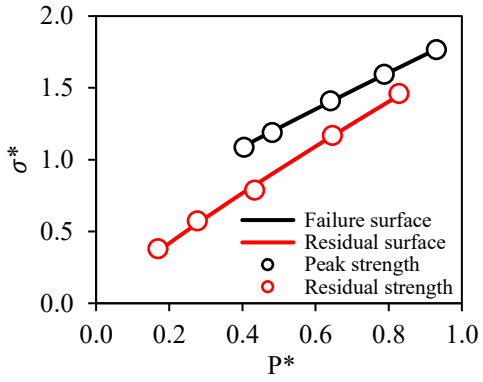


**Fig 4. Determination of the strength-related parameters of the RHT constitutive model for Jinping marble.**

$$\frac{1}{2} < Q_2 = Q_o + BP^* \leq 1 \tag{12}$$

Where: $Q_o$ and $B$ are the parameters of the RHT constitutive model. It should be noted that the tensile meridian corresponds to the triaxial extension stress state ($\sigma_1 = \sigma_2 \geq \sigma_3$), whereas the compressive meridian corresponds to the triaxial compression stress state ($\sigma_1 \geq \sigma_2 = \sigma_3$) [30]. In this section, experimental data from laboratory tests conducted by von Kármán, Böker and Ramsey, and Chester on similar marble, as collected by Yu and Ng, were used. These datasets are not specifically representative of Jinping marble. However, due to the limited availability of triaxial extension data for Jinping marble, data from other

marbles with mechanical properties similar to those of Jinping marble were utilized.

The tensile and compressive meridians, as well as their ratio, are shown in Fig. 5 [32]. The data used in Fig. 5 correspond to a minimum principal stress range of 25 MPa to 161.8 MPa for the compressive triaxial stress state, and a range of 60.5 MPa to 131.6 MPa for the extension stress state.

The RHT constitutive model parameters determined for Jinping marble are presented in Table 2.

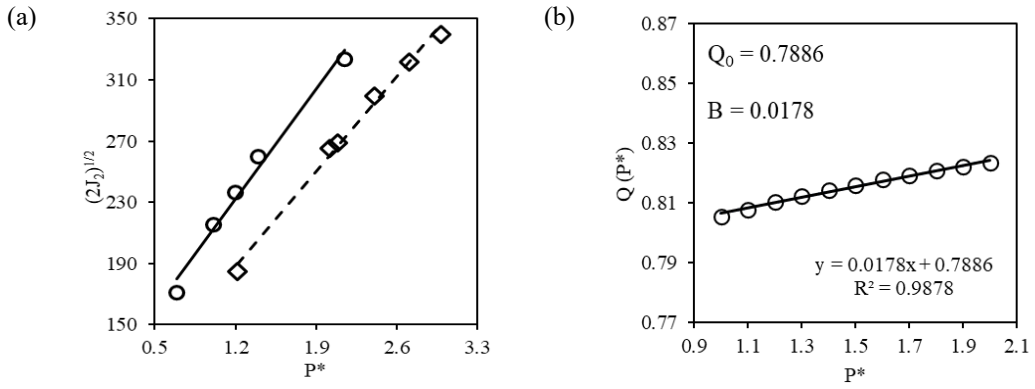


**Fig 5. Determination of the parameters for extending the compressive meridian of the RHT constitutive model to the three-dimensional surface for Jinping marble.**

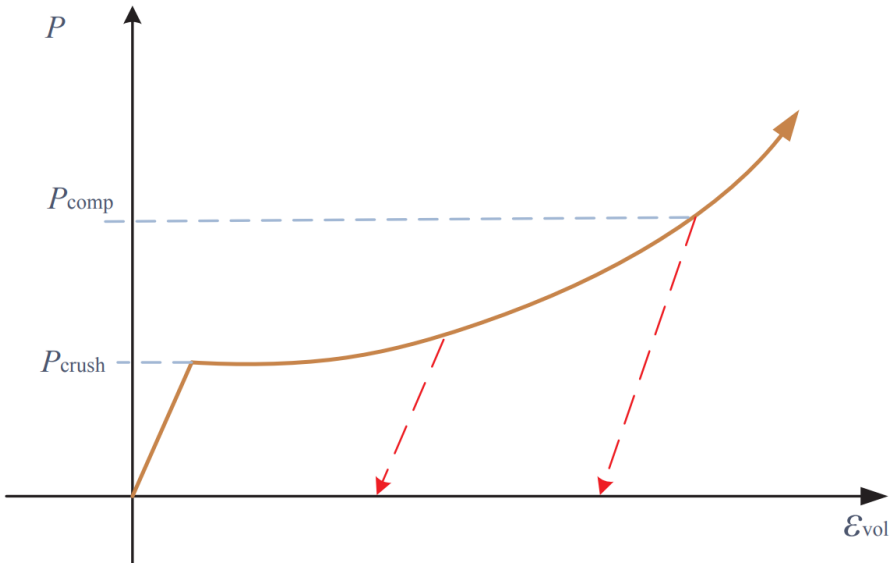


**Fig 6. The equation of state of the RHT constitutive model [30].**

**Table 2. The RHT constitutive model parameters determined for Jinping marble.**

| Parameter | Value | Parameter | Value | Parameter | Value | Parameter | Value |
|---|---|---|---|---|---|---|---|
| RO (kN/m$^3$) | 28 | FS* | 0.276 | $g_c^*$ | 0.85 | $A_f$ (1) | 1.464 |
| A | 1.464 | FT* | 0.0599 | $A_1$ (Gpa) | 36.7 | $N_f$ (1) | 0.8716 |
| n | 0.8716 | FC (Mpa) | 117 | $T_1$ (Gpa) | 36.7 | D1 | 0.02 |
| $A_f$ | 1.707 | B | 0.0178 | $T_2$ (Gpa) | 0 | D2 | 1 |
| $N_f$ | 0.8737 | $Q_o$ | 0.7886 | G (Gpa) | 22 | EPM | 0.005 |

(1) **These two parameters were determined via a calibration process.**

Where: RO denotes the intact rock density, FS* and FT* represent the shear and tensile strengths normalized with respect to the uniaxial compressive strength FC, respectively. The parameters $A_1$, $T_1$ and $T_2$ are the equation-of-state parameters for the compressive and tensile stress states and are taken to be equal to the bulk modules (Within this confining pressure range, the material behavior corresponds to the first (linear) phase of the equation of state. Consequently, this assumption holds true only for this phase). The parameter G denotes the shear modules, which is calculated using the Young's modules and

Poisson's ratio of Jinping marble. $g_c$* determines the ratio between the elastic limit surface and the peak strength surface. The final column of the table contains the calibrated parameters associated with the refinement of the post-failure behavior.

## III. Numerical Simulation

LS-Dyna software has been used for simulation in this study. The model comprises three finite element parts, including an upper jaw, a bottom jaw, and a cylindrical specimen between them and positioned under the load of the upper jaw. The specimen is meshed with 51,800 solid elements.

The upper and bottom jaw were fixed rotationally about the X, Y, and Z axes. They were also fixed translationally in all directions, except for the upper jaw, which is free to move in the Z direction. Therefore, the specimen was loaded through the displacement of the upper jaw.

The contact between the specimen and both the bottom and upper jaws was defined using the *CONTACT_AUTOMATIC_SURFACE_TO_SURFACE contact model.

## IV. Results and Discussion

In this section, the determined parameters for Jinping marble are defined in both the RHT and KCC constitutive models, and triaxial compression tests under confining pressures of 5, 20 and 40 MPa are simulated. The simulation results obtained using the KCC constitutive model are presented in Fig. 7.

### *B. KCC Constitutive Model Results*

According to the results illustrated in Fig. 7, the prediction error of the model in estimating the peak strength decreases as the confining pressure increases, from approximately 30% for the specimen subjected to a confining pressure of 5 MPa to less than 10% for the specimen under 40 MPa. However, the pre-failure rock behavior, including the slope of the linear elastic portion of the stress-strain curve, is predicted more accurately in the simulations conducted at lower confining pressures. It should also be noted that the post-peak slope of the stress–strain response and the residual strength at confining pressures 5 MPa and 40 MPa show reasonably good agreement with the laboratory test results. Nevertheless, none of the simulated cases under confining pressures of 5, 20 and 40 MPa were able to accurately predict the complete mechanical response of Jinping marble. Therefore, the KCC constitutive model did not provide satisfactory predictive performance.

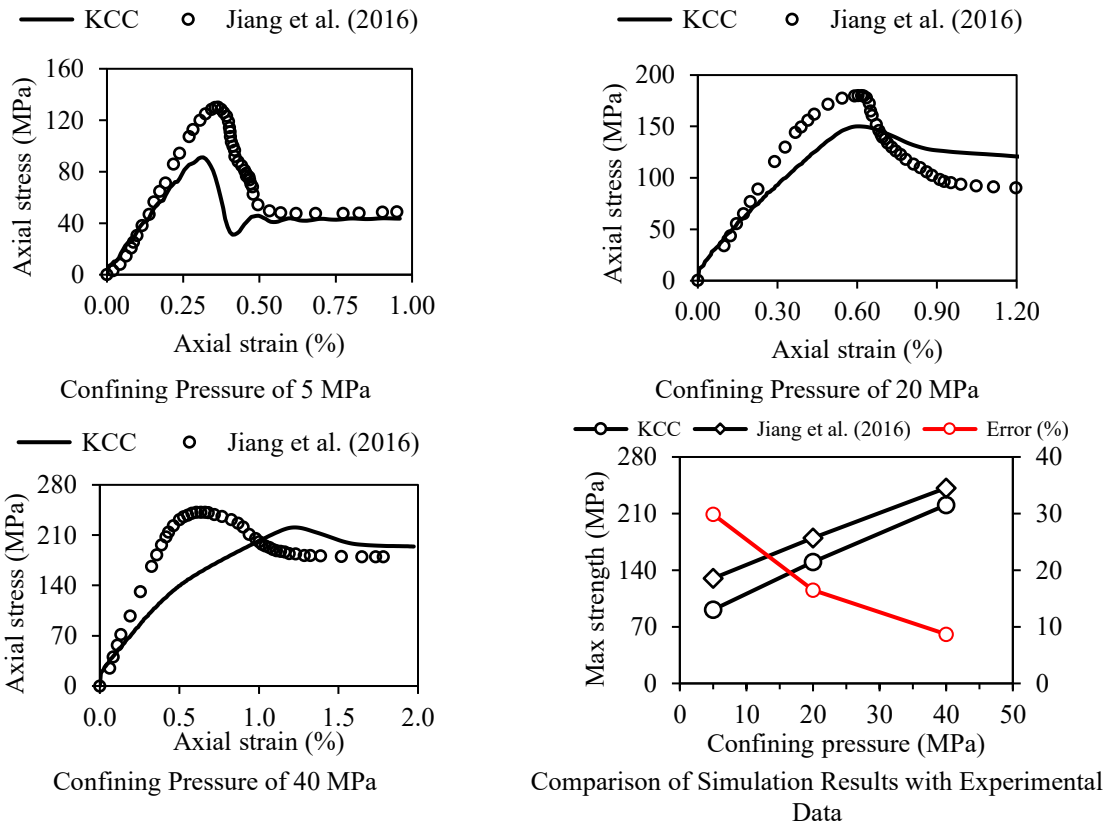


**Fig 7. Simulation Results of Triaxial Compressive Tests under Variable Confining Pressures Using the KCC Constitutive Model.**

### *A. RHT Constitutive Model Results*

The results of the triaxial compression test simulations under confining pressures of 5, 20 and 40 MPa using the RHT constitutive model are also shown in Fig. 8. The presented results reflect the outcomes of calibrating the model parameters that govern the post-

peak behavior and residual strength of Jinping marble. The calibration procedure was performed such that, after determining the parameters that could be obtained experimentally, the remaining parameters were refined through iterative adjustments and monitoring of the simulation results for a model under a confining pressure of 5 MPa. The calibrated model was then validated using other models subjected to higher confining pressures. It should be noted that this calibration procedure did not affect the prediction of the pre-peak behavior of the rock or the peak strength at the onset of failure. As shown in the Fig. 9, the simulation results obtained using the RHT constitutive model exhibit very good accuracy. The RHT constitutive model provides satisfactory performance in predicting the pre-failure behavior, the peak strength at the onset of failure, as well as the post-peak deformation and residual strength. The high fidelity of these results further confirms the validity of the parameter determination and calibration procedure adopted for this constitutive model. According to the peak strength error curve obtained from the comparison between the numerical and experimental results, the prediction error is less than 5% for the specimen subjected to a confining pressure of 5 MPa and less than 1% for the other two specimens.

### *C. Comparison of KCC and RHT Models*

Finally, Fig. 9 compares the peak strength values obtained under different confining pressures using the RHT and KCC constitutive models. The specimen is shown in Fig. 10 under a confining pressure of 5 MPa, simulated using the RHT constitutive model to demonstrate the model's ability to predict post-peak behavior and crack propagation.

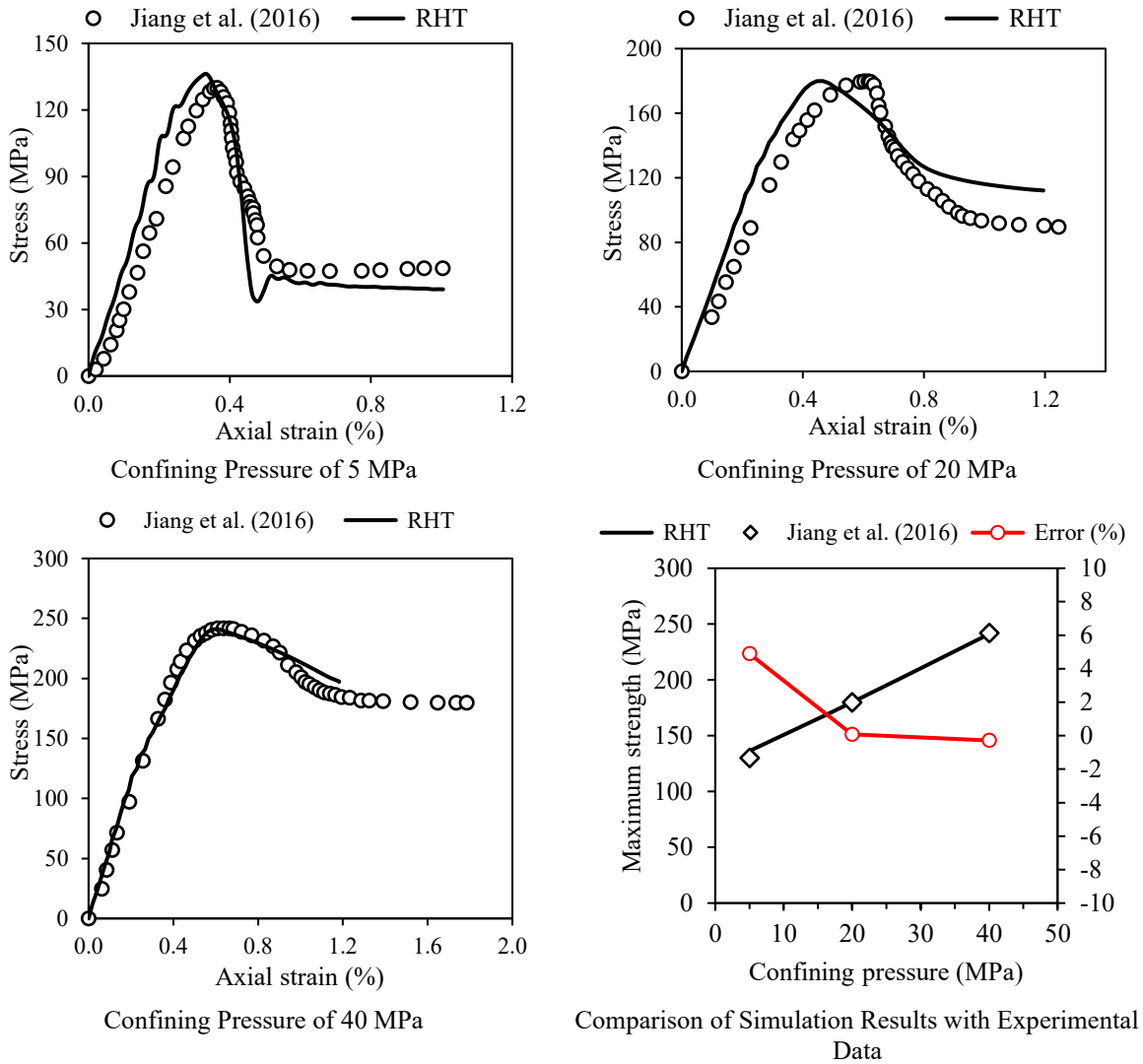


**Fig 8. Simulation Results of Triaxial Compressive Tests under Variable Confining Pressures Using the RHT Constitutive Model.**

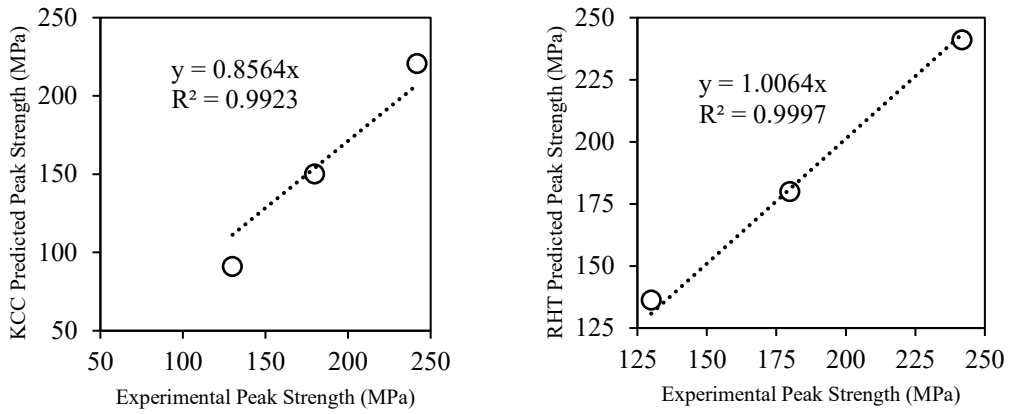


**Fig 9. Comparison of the RHT and KCC constitutive models in predicting peak strength under confining pressures of 5, 20, and 40 MPa.**

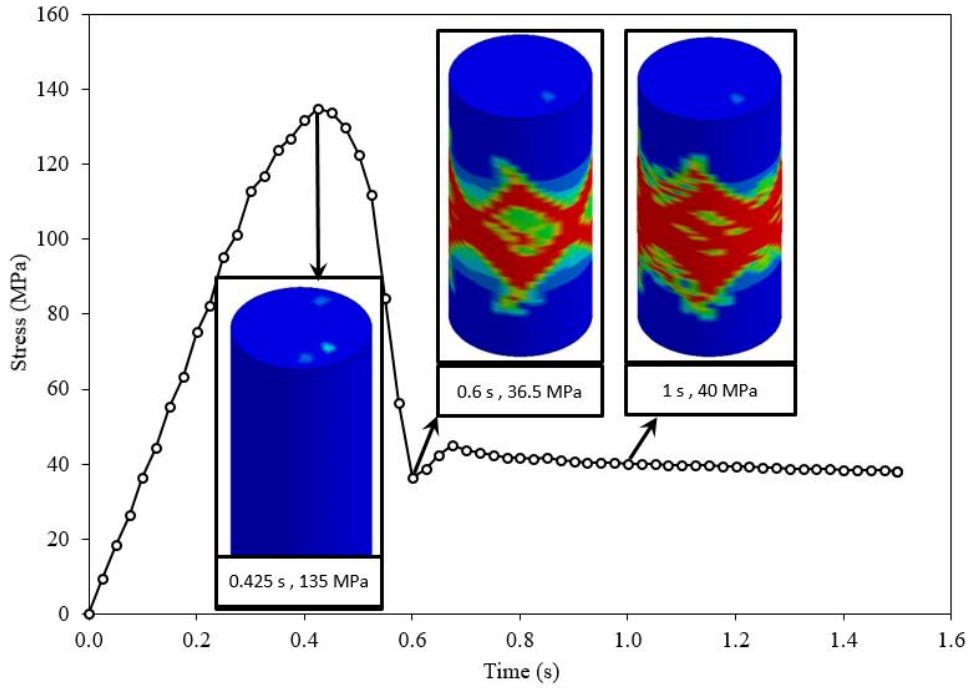


**Fig 10. Specimen simulated by RHT model under 5 MPa confining pressure.**

## V. CONCLUSION

This study evaluated the predictive performance of the RHT and KCC constitutive models in simulating the mechanical behavior of Jinping marble under conventional triaxial stress conditions. Both models were first briefly introduced, and their respective model parameters were determined specifically for Jinping marble. Numerical simulations of triaxial compression tests were performed at confining pressures of 5, 20, and 40 MPa, and the results were compared with experimental observations to assess the accuracy of each model in predicting the rock's mechanical response.

The KCC model demonstrated limited predictive capability for Jinping marble. While the model's prediction of peak strength improved with increasing confining pressure—from approximately 30% error at 5 MPa to less than 10% at 40 MPa—the pre-failure behavior, particularly the slope of the elastic portion of the stress–strain curve, was more accurately captured at lower confining pressures. The post-peak response and residual strength predicted by the KCC model exhibited reasonable agreement with experimental data at selected confining pressures. However, the model failed to reproduce the complete mechanical response across all tested conditions, highlighting its limitations for accurately simulating the full stress-strain behavior of Jinping marble.

In contrast, the RHT constitutive model provided consistently high-fidelity predictions across all confining pressures. The calibration procedure, involving both experimentally determined parameters and iterative refinement of remaining parameters, allowed the model to accurately capture the pre-failure behavior, peak strength at failure onset, and post-peak

deformation, including residual strength. The numerical results showed excellent agreement with laboratory data, with peak strength prediction errors less than 5% at 5 MPa and below 1% for the higher confining pressures. These findings demonstrate that the RHT model is capable of accurately representing both the elastic and post-failure response of Jinping marble, including the effects of confining pressure on strength and deformation.

Overall, the comparative analysis indicates that while both models are suitable for simulating rock behavior under triaxial conditions, the RHT model outperforms the KCC model in terms of overall predictive accuracy, particularly for capturing post-peak softening and residual strength. Therefore, for Jinping marble, the RHT model is recommended as the preferred constitutive formulation for numerical simulations requiring accurate representation of both pre- and post-failure behavior.

These results not only validate the parameter determination and calibration procedures adopted for the RHT model but also provide a framework for selecting appropriate constitutive models for brittle rock types in numerical analyses. The findings highlight the importance of accurately capturing post-peak behavior and residual strength in constitutive modeling, particularly when simulating rock under varying confining pressures. Future studies may extend this approach to other rock types and stress conditions, further improving the reliability of numerical predictions in rock mechanics and engineering applications.

## REFERENCES


[1] Q. B. Zhang and J. Zhao, “A review of dynamic experimental techniques and mechanical behaviour of rock materials,” Rock Mech. rock Eng., vol. 47, no. 4, pp. 1411–1478, 2014.

[2] G. R. Johnson and T. J. Holmquist, “A computational constitutive model for brittle materials subjected to large strains, high strain rates, and high pressures,” in Shock wave and high-strain-rate phenomena in materials, CRC Press, 2023, pp. 1075–1082.

[3] G. R. Johnson and T. J. Holmquist, “An improved computational constitutive model for brittle materials,” in AIP conference proceedings, American Institute of Physics, 1994, pp. 981–984.

[4] H. A. Ai and T. J. Ahrens, “Simulation of dynamic response of granite: A numerical approach of shock-induced damage beneath impact craters,” Int. J. Impact Eng., vol. 33, no. 1–12, pp. 1–10, 2006.

[5] H. Huang, W. Li, and Z. Lu, “Determination of parameters of Johnson-Holmquist-II (JH-2) constitutive model for red sandstone,” in Journal of Physics: Conference Series, IOP Publishing, 2021, p. 012071.

[6] M. A. Karasev, R. O. Sotnikov, V. Y. Sinegubov, N. A. Egorova, K. V Makarov, and A. I. Thorikov, “Development of a model for predicting the dynamic effect on the stability of rock excavation,” in Journal of Physics: Conference Series, IOP Publishing, 2019, p. 012051.

[7] G. W. Ma and X. M. An, “Numerical simulation of blasting-induced rock fractures,” Int. J. Rock Mech. Min. Sci., vol. 45, no. 6, pp. 966–975, 2008.

[8] M. M. D. Banadaki and B. Mohanty, “Numerical simulation of stress wave induced fractures in rock,” Int. J. Impact Eng., vol. 40, pp. 16–25, 2012.

[9] F. Zhu and J. Zhao, “Peridynamic modelling of blasting induced rock fractures,” J. Mech. Phys. Solids, vol. 153, p. 104469, 2021.

[10] P. Baranowski, M. Kucewicz, M. Pytlik, and J. Małachowski, “Shock-induced fracture of dolomite rock in small-scale blast tests,” J. Rock Mech. Geotech. Eng., vol. 14, no. 6, pp. 1823–1835, 2022.

[11] F. Ren, T. Fang, and X. Cheng, “Study on rock damage and failure depth under particle water-jet coupling impact,” Int. J. Impact Eng., vol. 139, p. 103504, 2020.

[12] T. J. Holqmuist, G. R. Johnson, and W. Cook, “A computational constitutive model for concrete subjected to large strains, high strain rate, and high pressures,” in 14th international symposium on ballistics, 1993, pp. 591–600.

[13] M. Kucewicz, P. Baranowski, and J. Małachowski, “Dolomite fracture modeling using the Johnson-Holmquist concrete material model: Parameter determination and validation,” J. Rock Mech. Geotech. Eng., vol. 13, no. 2, pp. 335–350, 2021.

[14] B. Xie, Z. Yan, Y. Du, Z. Zhao, and X. Zhang, “Determination of Holmquist–Johnson–Cook constitutive parameters of coal: laboratory study and numerical simulation,” Processes, vol. 7, no. 6, p. 386, 2019.

[15] Y. Liu, J. Wei, and T. Ren, “Analysis of the stress wave effect during rock breakage by pulsating jets,” Rock Mech. Rock Eng., vol. 49, no. 2, pp. 503–514, 2016.

[16] B. Xie, D. Chen, H. Ding, G. Wang, and Z. Yan, “Numerical Simulation of Split-Hopkinson Pressure Bar Tests for the Combined Coal-Rock by Using the Holmquist–Johnson–Cook Model and Case Analysis of Outburst,” Adv. Civ. Eng., vol. 2020, no. 1, p. 8833233, 2020.

[17] L. J. Malvar and D. Simons, “Concrete material modeling in explicit computations,” in Proceedings, workshop on recent advances in computational structural dynamics and high performance computing, USAE waterways experiment station, Vicksburg, MS, 1996, pp. 165–194.

[18] L. J. Malvar, J. E. Crawford, J. W. Wesevich, and D. Simons, “A plasticity concrete material model for DYNA3D,” Int. J. Impact Eng., vol. 19, no. 9–10, pp. 847–873, 1997.

[19] M. Kucewicz, P. Baranowski, and J. Małachowski, “Determination and validation of Karagozian-Case Concrete constitutive model parameters for numerical modeling of dolomite rock,” Int. J. Rock Mech. Min. Sci., vol. 129, p.

104302, 2020.
[20] A. Mardalizad, M. Caruso, A. Manes, and M. Giglio, “Investigation of mechanical behaviour of a quasi-brittle material using Karagozian and Case concrete (KCC) model,” J. Rock Mech. Geotech. Eng., vol. 11, no. 6, pp. 1119–1137, 2019.
[21] A. Mardalizad, T. Saksala, A. Manes, and M. Giglio, “Numerical modeling of the tool-rock penetration process using FEM coupled with SPH technique,” J. Pet. Sci. Eng., vol. 189, p. 107008, 2020.
[22] Y. Tian, Y. Sang, and J. Liu, “A numerical model for rock cutting with diamond circular saw blade based on smoothed particle galerkin method,” Math. Probl. Eng., vol. 2022, no. 1, p. 2036301, 2022.
[23] M. Kucewicz, P. Baranowski, Ł. Mazurkiewicz, and J. Małachowski, “Comparison of selected blasting constitutive models for reproducing the dynamic fragmentation of rock,” Int. J. Impact Eng., vol. 173, p. 104484, 2023.
[24] W. Riedel, K. Thoma, S. Hiermaier, and E. Schmolinske, “Penetration of reinforced concrete by BETA-B-500 numerical analysis using a new macroscopic concrete model for hydrocodes,” in Proceedings of the 9th International Symposium on the Effects of Munitions with Structures, Berlin-Strausberg Germany, 1999, pp. 315–322.
[25] H. Rouhani, M. Arash, and E. Farrokh, “Investigating the effects of confining pressure and loading rate on damage propagation and mode I stress intensity factor of granite using the RHT constitutive model,” Geomech. Geophys. Geo-Energy Geo-Resources, vol. 11, no. 1, p. 79, 2025.
[26] H. Rouhani and E. Farrokh, “Failure analysis of Nehbandan granite under various stress states and strain rates using a calibrated Riedel–Hiermaier–Thoma constitutive model,” Geomech. Geophys. Geo-Energy Geo-Resources, vol. 10, no. 1, p. 157, 2024.
[27] Q. Jiang, S. Zhong, J. Cui, X.-T. Feng, and L. Song, “Statistical characterization of the mechanical parameters of intact rock under triaxial compression: an experimental proof of the Jinping marble,” Rock Mech. Rock Eng., vol. 49, no. 12, pp. 4631–4646, 2016.
[28] Z. Liu and J. Shao, “Strength behavior, creep failure and permeability change of a tight marble under triaxial compression,” Rock Mech. Rock Eng., vol. 50, no. 3, pp. 529–541, 2017.
[29] Z. Wang, S. Li, J. Wang, F. Xiong, and L. Xie, “Mechanical behavior, mesoscopic properties and energy evolution of deeply buried marble during triaxial loading,” Int. J. Damage Mech., vol. 31, no. 10, pp. 1592–1612, 2022.
[30] L. X. Xie, W. B. Lu, Q. B. Zhang, Q. H. Jiang, M. Chen, and J. Zhao, “Analysis of damage mechanisms and optimization of cut blasting design under high in-situ stresses,” Tunn. Undergr. Sp. Technol., vol. 66, pp. 19–33, 2017.
[31] C. Grunwald, B. Schaufelberger, A. Stolz, W. Riedel, and T. Borrvall, “A general concrete model in hydrocodes: verification and validation of the Riedel–Hiermaier–Thoma model in LS-DYNA,” Int. J. Prot. Struct., vol. 8, no. 1, pp. 58–85, 2017.
[32] H. Yu and K. Ng, “Analytical model for failure strength of brittle rocks under triaxial compression and triaxial extension,” Int. J. Geomech., vol. 22, no. 4, p. 06022003, 2022.

نشریه‌ی مکانیک سنگ
JOURNAL OF ROCK MECHANICS
دوره نهم، شماره۴، زمستان ۱۴۰۴، صفحه ۳۳ تا ۴۳
https://doi.org/10.22034/IRSRM.2026.578065.1075

# مقایسه عملکرد مدل‌های رفتاری RHT و KCC در پیش‌بینی رفتار سنگ مرمر جینپینگ تحت بارگذاری استاتیکی و شبه‌استاتیکی

**هومن روحانی[۱]، آیدا عاملی قمصر[۱]، ابراهیم فرخ[۱*]**
۱- دانشکده مهندسی معدن، دانشگاه صنعتی امیرکبیر، تهران، ایران.

**دریافت : ۱۴۰۴/۱۱/۰۱؛ پذیرش: ۱۴۰۴/۱۲/۲۹**
**(*نویسنده مسئول: e.farrokh@aut.ac.ir)**

**چکیده**

در این مطالعه، عملکرد مدل‌های رفتاری *RHT* و *KCC* در زمینه شبیه‌سازی رفتار مکانیکی سنگ مرمر جینپینگ مورد ارزیابی و مقایسه قرار گرفته است. در ابتدا، مدل‌های شکست و معادلات حالت هر کدام از مدل‌های رفتاری مذکور به طور مختصر شرح داده شده است. سپس، آن گروه از پارامترهای هر مدل که به منظور شبیه‌سازی رفتار سنگ مذکور تحت بارگذاری سه‌محوری استاتیکی مورد نیاز بوده تعیین شده است. آزمون مقاومت فشاری سه‌محوری مرسوم تحت فشارهای جانبی ۵، ۲۰ و ۴۰ مگاپاسکال، با استفاده از هر دو مدل رفتاری، شبیه‌سازی شده و نتایج حاصل از شبیه‌سازی عددی با نتایج حاصل از داده‌های آزمایشگاهی موجود از سنگ مورد مطالعه، مقایسه شده است. مطابق نتایج حاصله، پیشبینی مقادیر مقاومت حداکثر و تغییرشکل‌پذیری سنگ پیش از شکست، توسط مدل رفتاری *RHT* بهتر پیشبینی شده است. بنابرین، مدل رفتاری *RHT* به عنوان مدل تواناتر و ارائه دهنده پیشبینی با صحت بیشتر تشخیص داده شده و رفتار پس از شکست سنگ، برای این مدل از طریق فرایند کالیبراسیون، تدقیق شده است.

**واژگان کلیدی** مدل رفتاری، مرمر جینپینگ، RHT، KCC